SM Report 92-3

On the Dependence of the Dynamic Crack Tip Temperature Fields in Metals Upon Crack Tip Velocity and Material Parameters

J.J. Mason[a]
A.J. Rosakis[b]

Graduate Aeronautical Laboratories
California Institute of Technology
Pasadena, CA 91125

[a] Graduate Research Assistant

[b] Associate Professor

On the Dependence of the Dynamic Crack Tip Temperature Fields in Metals Upon Crack Tip Velocity and Material Parameters[a]

James J. Mason and Ares J. Rosakis

California Institute of Technology, 105-50, Pasadena,CA 91125

Abstract

Although various approximations have been used to analytically predict the temperature rise at a dynamic crack tip and its relation to the crack tip velocity or the material properties, few experimental investigations of these effects exist. Here, the method of using a high speed infrared detector array to measure the temperature distribution at the tip of a dynamically propagating crack tip is outlined, and the results from a number of experiments on different metal alloys are reviewed. First the effect of crack tip velocity is reviewed, and it is seen that the maximum temperature increases with increasing velocity and that a significant change in the geometry of the temperature distribution occurs at higher velocities in steel due to the opening of the crack faces behind the crack tip. Next, the effect of thermal properties is examined, and it is seen that, due to adiabatic conditions at the crack tip, changes in thermal conductivity do not significantly affect the temperature field. Changes in density and heat capacity are more likely to produce significant differences in temperature than changes in thermal conductivity. Finally, the effect of heat upon the crack tip deformation is reviewed, and it is seen that the generation of heat at the crack tip in steel leads to the formation of a shear band at 45° to the surface of the specimen. In titanium, no conclusive evidence of shear band formation is seen.

[a] Research performed with support from the Office of Naval Research under grant N00014-90-J-1340.

1. Introduction

It is known that in ductile metals plasticity ahead of a dynamically propagating or dynamically loaded crack can lead to the generation of heat resulting in a significant temperature rise at the crack tip. Such increases in thermal energy can lead to changes in fracture toughness, changes in fracture mode and instabilities in the resulting deformation. For example, it has been observed that heat generated in dynamic deformations can result in the decomposition of thermally unstable materials(Fox and Sonria-Ruiz, 1970) and localized melting in titanium alloys(Bryant et al., (1986). If the conditions of the deformation are approximated by neglecting heat conduction (by assuming that adiabatic heating conditions prevail) and by neglecting the thermo-elastic effect, the temperature rise due to dynamic plasticity is given quite simply by

$$\Delta T(t) = \frac{1}{\rho c_p} \int_{-\infty}^{t} \beta \sigma_{ij}(\tau) \dot{\epsilon}^p_{ij}(\tau) d\tau \tag{1}$$

where $\Delta T(t)$ is the temperature rise, β is the fraction of work converted to heat—roughly .85-1.00, (Taylor and Quinney, 1934; Bever et al., 1973)—ρ is the density (assumed independent of temperature), c_p is the specific heat (also assumed independent of temperature), and σ_{ij} and $\dot{\epsilon}^p_{ij}$ are the cartesian stress and plastic strain-rate tensor components. The temperature field in this case corresponds exactly with the plastic deformation field; when the plastic work density is higher the temperature is higher, and there is no temperature rise at a point if no plasticity occurs there.

While the assumption of adiabatic heating and the negligence of the thermo-elastic effect may significantly simplify the problem of calculating the temperature rise in dynamic deformation experiments, the conduction of heat is not completely absent in any realistic situation and elasticity is always present. If the effects of heat conduction and thermo-elasticity are included in the analysis, the standard heat (or diffusion) equation is invariably invoked,

$$\alpha \nabla^2 T - \frac{\partial T}{\partial t} = -\frac{\dot{W}^p}{\rho c_p} + \frac{\kappa}{\rho c_p} \frac{E}{(1-2\nu)} T_o \dot{\epsilon}^e_{kk} \tag{2a}$$

where $\alpha = k/\rho c_p$, k is the thermal conductivity,

$$\dot{W}^p = \beta \sigma_{ij} \dot{\epsilon}^p_{ij}. \tag{2b}$$

T_o is the initial, ambient temperature, κ is the thermal expansion coefficient, E is Young's modulus, ν is Poisson's ratio, and $\dot{\epsilon}^e_{kk}$ is the rate of elastic dilatation. On the right hand side

of this equation are two terms characterizing two sources of heat in a deformation; the first term characterizes heat generated by plastic deformation (Taylor and Quinney, 1934: Bever et al., 1973) while the second term characterizes thermo-elastic cooling due to elastic dilatation (Sneddon and Berry, 1958). The solution of this coupled heat equation is greatly dependent upon the geometry of the problem at hand. For a crack of length a, propagating at a constant velocity, $\dot{a}$, it is beneficial to use a coordinate system that is translating with the crack tip. This results in a reformulation of Eq (2a);

$$\alpha \nabla^2 T + \dot{a}\frac{\partial T}{\partial x_1} = -\frac{\dot{W}^p}{\rho c_p} \tag{3}$$

where thermo-elastic effects have been neglected, x_1 is the coordinate parallel to the crack faces and x_2 is perpendicular to the crack faces with the origin at the crack tip. The solution of Eq (3) for a point source of heat in two dimensions is given by Carslaw and Jaeger (1959) as

$$T_p(x_1, x_2) = \frac{\dot{Q}}{2\pi k}\exp\left[-\frac{\dot{a}x_1}{2\alpha}\right] K_0\left(\frac{\dot{a}r}{2\alpha}\right) \tag{4}$$

where $r = \sqrt{x_1^2 + x_2^2}$ and K_0 is the modified Bessel's function of the zeroth order. To predict the temperature field around a propagating crack tip the point source solution is used as a Green's function to be integrated over the area of the plastic work zone, A_p. Assuming the plastic work zone is self-similar throughout the thickness of the specimen and letting $\dot{Q} = \dot{W}^p d\xi_1 d\xi_2$, the temperature field due to a experimental plastic zone is given by

$$T(x_1, x_2) = \int_{A_p} T_p(x_1 - \xi_1, x_2 - \xi_2)\dot{W}^p(\xi_1, \xi_2) d\xi_1 d\xi_2. \tag{5}$$

Because of the logarithmic singularity of the modified Bessel's function at $r = 0$, the solution given by Eq (5) is finite and well behaved. Note that the assumption of a through-thickness, self-similar plastic work zone is rarely true where experimental temperature measurements are made—at the surface—due to the stress free surface boundary condition. Also note that knowledge of the active plastic zone size and shape, $\dot{W}^p(x_1, x_2)$. is required in Eq (5). Exactly determining this function in closed form for most real materials is virtually impossible. Approximations are used, or numerical calculation are substituted.

Dynamic Crack Tip Temperature Fields

In order to apply Eq (1) or Eq (5) to known problems—that is, in order to exactly determine the extent of heating and the shape of a temperature field for known dynamic loading—a constitutive equation is required to specify a relation between stress, σ_{ij}, temperature, T, strain, ϵ_{ij}, and strain-rate $\dot{\epsilon}_{ij}$. This constitutive law would be used in Eq (2b) in conjunction with Eqs (1) or (5) to find the temperature field solution. Specifically lacking in the studies of dynamic deformation and heat generation are investigations of the constitutive behavior of materials. The dependence of stress upon temperature in not easily quantified; it is known that the rate of heating can have significant effects making it experimentally difficult to test at high temperatures. Also, the dependence of stress upon strain and temperature is associated with the history of temperature and strain as well as their current value. (It is well known that thermo-mechanical treatment can drastically alter the response of the material.) Furthermore, in dynamic testing arrangements such as the split Hopkinson bar (Follansbee, 1985) or plate impact tests (Clifton and Klopp, 1985), where dynamic constitutive laws are usually investigated experimentally, the temperature is not known and, in fact, effects attributed to a change in strain-rate could very well be due to heating. This leaves an investigator with little hope of precisely modelling the temperature field in most experimental situations. Theorists are forced to *assume* a constitutive relation, usually a general one to incorporate most possibilities, and produce results for purely theoretical materials. Fortunately, for metals some common characteristics may be included in the constitutive law to qualitatively reproduce experimental behavior. First, most metals work-harden; with increasing plastic strain the resistance of the material to further plastic strain increases. Second, many metals strain-rate harden; increasing the plastic strain-rate results in increased resistance to further plastic straining. And, lastly, most metals thermally soften; increasing the temperature results in a decrease in the resistance to further plastic straining.

A number of theoretical investigations have taken the approach outlined above by directly assuming a constitutive law or by assuming a shape and size for the dynamic plastic zone at a crack tip. In most calculations the emphasis is placed upon calculating the maximum temperature so that it can be ascertained as to whether heating effects are important. Decoupled mechanical and thermal fields are usually evaluated. Rice and Levy (1969) assumed a Dugdale plastic zone where all the plastic work is confined to the x_1 axis ahead of the crack tip. By assuming a dynamic stress intensity factor, K_I^d, a crack speed, the yield stress and the thermal properties of the material, they were able to calculate significantly high values for the maximum temperature,

T_{max}. For mild steel they predict 1400°C at a crack speed of 900 m/s and for titanium they predict the temperature will be twelve times as high as that for steel. Sung and Achenbach (1987) used the constitutive law for visco-plastic, Bodner-Partom materials in a plane strain approximation to estimate the work zone from dynamic fracture theory and find the maximum temperature under adiabatic conditions. They indicate temperatures as high as 700°C for a crack propagating at a velocity of 300 m/s in steel. Kuang and Alturi (1985) used a moving finite element calculation procedure in which the plastic work rate was distributed uniformly or in a $1/r$ distribution. The magnitude of the plastic work is linearly related to crack velocity. They estimated $T_{max} \approx 700$°C in steel at a velocity of 762 m/s. Douglas and Mair (1987) used asymptotic fields in Mode-III dynamic crack propagation in an elastic-perfectly plastic material. They predict temperature rises on the order of 1°C in steel and 50°C in titanium for a crack propagating at 1500 m/s. Malali (1988) used finite elements in a Mode-III loading to calculate the plastic work field for an elastic-perfectly plastic material resulting in maximum temperatures of 528°C in steel at 1500 m/s and 11500°C in titanium at 1500 m/s. Krishna, Narasimhan and Prabhaker (1991) used plane strain, steady state crack propagation in a visco-plastic material to calculate the active plastic zone. Assuming all the work is dissipated as heat they find maximum temperatures in the range 160°C to 400°C for various material parameters with a crack propagating at 300 to 1500 m/s. For a Mode-III crack in glass Li et al. (1988) found the temperature field based on the crack tip plastic zone solution of Chitaley and McClintock. The maximum temperature calculated in this manner is 540°C at 200 m/s. It should be noted that there is a sensitivity of the maximum temperature to the shape of the active plastic zone in the above calculations. By changing the plastic work rate distribution large differences in the maximum temperature may be induced. However, it suffices to say that temperature rises at the crack tip are expected to be significant.

Weichert and Schönert(1974, 1978a, and 1978b) have produced the temperature fields, and not just the maximum temperature, for square plastic work zones, as well as circles, of constant intensity. They predict temperatures rises of 3000°C for brittle materials such as quarts and glass by using a direct numerical integration technique to evaluate Eq (5). For the case of a propagating crack in metals the theoretical temperature field calculated by the same method for an experimental approximation of the plastic work zone (Mason and Rosakis, 1992) is shown in Fig 1. Notice that the contours of constant temperature extend straight back from the theoretical

plastic zone eventually curving toward the negative x_1 axis some distance behind the crack tip. This solution differs from the adiabatic solution in that the temperature is forced to zero at $r = \infty$ due to the boundary conditions of the point source solution in Eq (4).

There has been some suggestion that hyperbolic heat conduction may play a factor when crack speeds become significant with respect to the shear wave speed in the material (Tzou, 1990a and 1990b). However, closer examination shows that the simplified theory of hyperbolic heat conduction produces the same prediction as seen in Fig 1 for typical experimental conditions and crack speeds below the wave speed of heat propagation. When the crack speed is above the wave speed of heat propagation hyperbolic heat conduction theory predicts a temperature field that is drastically different than the experimentally observed fields (Mason and Rosakis, 1992).

While most of the investigations mentioned above include work hardening in the constitutive equation, few include strain-rate hardening or visco-plasticity, and none include thermal softening. It is thermal softening that commonly produces instabilities and anomalous behavior in dynamic plasticity experiments. As in a standard uniaxial tension test where geometric softening (due to the reduction in area of the test sample) competes with the inherent work hardening of the material until an instability, a neck, results, in dynamic tests thermal softening competes with work hardening and strain-rate hardening. In a dynamic plasticity test the generation of heat, which increases the temperature, T, can increase the amount of softening until an instability occurs resulting in the localization of the deformation to a single plane and the formation of a shear band. Adiabatic shear band formation has been observed for decades; for a review of the subject see Hutchinson (1984). In a torsional split hopkinson bar experiment, Duffy and coworkers (Marchand and Duffy, 1988; Hartley et al., 1987; and Duffy 1984) and Giovanola (1988a and 1988b) were able to form shear bands in pure shear on several steels. They observed two stages of shear and temperature localization. First, localization by means of a thermal instability model is observed. This localization is due to the competition between thermal softening and strain or strain-rate hardening. Next, localization occurs on a smaller scale related to microvoid formation and coalescence. Using infrared detectors, temperatures as high as 450°C have been measured in the shear bands (Marchand and Duffy, 1988; Hartley et al., 1987; and Duffy 1984).

2. Experimental Methods

The measurement of the temperature field at a dynamic crack tip (a crack tip that is either

propagating or dynamically loaded) requires some specific properties from the measurement apparatus. First, it is necessary that the measurement technique does not significantly alter the deformation field or the temperature field. Thus, it must be a non-destructive technique; drilling a hole for a thermocouple, for example, is not feasible. Second, it is necessary that the system be capable of fast response times. For a crack propagating at 900 m/s the temperature could rise from zero to its maximum in 2 μs. A rise time of at least 1 μs in the measuring system is required. Candidate methods include; thermocouples on the surface, thermally sensitive films and infrared detector.

Thermocouples have been used by Fuller et al. (1975), Shockey et al. (1983), Klemm (1989) and Döll (1973) to make some measurements involving the temperature fields around dynamically propagating cracks. In studying PMMA, Doll attached thermocouples within one millimeter of the crack path, and, as the crack passed, a temperature was recorded. Shockey et al. also used thermocouples welded to the side of the prospective crack path. Fuller et al. combined thermocouples with temperature sensitive liquid crystal films and infrared temperature measurements, using InSb detectors, of the crack faces. Eq (1) was used along with extensive assumptions about the plastic zone to find the maximum temperature, T_{max}=230°C. Klemm used the thermocouples in the crack path to actually measure the temperature field in the 50 mm plastic zone for a ductile steel. A maximum temperature of 100°C is reported.

Coffey and Jacobs (1981) and Swallowe et al. (1986) used thermally sensitive films to measured the temperature of various polymers under impact loading and subsequent failure. Temperatures up to 700°C are reported.

Moss and Pond (1975) used infrared detectors to investigate the formation of inhomogeneities in the deformation of copper. Although other authors had used unfocused IR detectors to measure average temperature (Fuller et al., 1975), Moss and Pond were interested in the formation of Luders bands in copper and, thus, they were interested in measuring the local thermal changes in the material. They used a single GeCu infrared detector in conjunction with a Cassegrain mirror system to measure temperature at two close points on the sample relative to each other. They report a temperature rise of 18°C in the Luders band compared to the bulk. Duffy and coworkers (Marchand and Duffy, 1988; Hartley et al., 1987; and Duffy 1984) used a linear array of InSb detectors focused with a single convex mirror, later replaced by a Cassegrain microscope objective, to measure the temperature in dynamically shearing cylinders

loaded in torsion. Maximum temperatures of 450°C are reported. The use of mirror elements in the optical systems by these authors is motivated by the desire to limit aberration. Because the detectors integrate energy over a wide range of wavelengths, it is necessary that the optical system focuses over that same range of wavelengths. Any refracting element would certainly produce unacceptable levels of chromatic aberration that would render the system inaccurate. The switch by Duffy and coworkers (Marchand and Duffy, 1988; Hartley et al., 1987; and Duffy 1984) and Fuller et al. (1975) to InSb detectors from the GeCu detector of Moss and Pond (1975) reflects the desire to produce the greatest sensitivity in the range of wavelengths expected in addition to maintaining the smallest rise time possible. InSb offers the best balance of these two objectives.

The difficulty with thermocouples is that they produce very small signals even when placed within 1mm of the crack path. Locating them directly in the crack path would still not suffice unless very large plastic zones were expected as in the case of Klemm (1989). Also, because of the finite size of the actual thermocouple junction, slow rise times, $> 1\mu s$, are characteristic. Thermally sensitive films suffer from calibration difficulties. The duration and temperature of exposure *both* contribute to the darkening of the film. It is necessary to assign a temperature value to various grey levels in a calibration before any quantitative results may be recorded, and there is always some ambiguity due to the effects of the length of exposure. Furthermore, both thermocouples and thermally sensitive films do not offer high spatial resolution. It is expected from Fig 1 that the temperature will be localized to a small area, thus thermocouple measurements are taken some distance away from the maximum temperature and extrapolation is used. Thermally sensitive films blacken in the area of maximum temperature making the indiscernible grey level patterns. Finally, thermocouples and thermally sensitive films offer only surface temperature measurements. No indication of the temperature within the solid is recorded. Infrared detectors offer an easy, but expensive, solution to the problems of measuring the temperature field at a crack tip with thermocouples or thermally sensitive films. Infrared detectors have fast response times, are non-destructive and are relatively easy to calibrate and utilize. One drawback to using infrared detectors, however, is that they too offer only surface temperature measurement.

The results reported here use the system employed by Zehnder and Rosakis (1991 and 1992) and Zehnder and Kallivayalil (1991). An Offner imaging system is used, instead of a Cassegrain

system, in conjunction with a linear array of InSb detectors. Originally developed for use in micro-lithography,(Offner, 1975) the Offner optical system offers the ability to correct the image for third and fifth order abberations. Although such accuracy may not be required due to the finite detector size, the system is quite simple to set up, and it offers some desirable features. First, the system can be easily and inexpensively assembled from commercially available optical components. Suzuki (1983a and 1983b) has evaluated the proper separation distance of the two reflecting components that minimizes the abberations. Second, by choosing large components the system can be set up with a large aperture making the detection of small changes in temperature quite easy. Also, for the temperature measurement around dynamically propagating crack tips it is desirable to have the measuring equipment a safe distance from the fracture event. The Offner system can accommodate this requirement without difficulty. One drawback to the Offner system is that it has fixed magnification, 1:1, that cannot be changed without destroying the performance of the optical system. Also, the image is not formed on the system axis, and the use of planar mirrors is required to make the image easily accessible. In contrast to the Offner system, the Cassegrain system *can* be used to produce variable magnification, and the detector array may be placed in line with the system so that no additional planar mirrors are required to view the image. However, drawbacks to the Cassegrain system include; obstructed aperture, small field of view and less aberration correction than the Offner system. Furthermore, the system is expensive if it is purchased commercially. There are several additional promising optical systems in the literature that provide a balance of the desirable features of both the Offner and the Cassegrain system(Rah and Lee, 1989, and Egdall, 1985). These systems use reflecting elements exclusively to eliminate chromatic aberration and have been corrected to produce almost diffraction limited performance. Unfortunately, they are not commercially available and require considerable sophistication to manufacture and assemble.

As noted before, the detectors integrate over a range of wavelengths. For InSb that range is 1 μm to 5.5 μm. The voltage produced by the detectors is related to the energy emitted by the specimen through an integral depending upon the emissivity of the material, $\epsilon(\lambda, T)$, the spectral response of the InSb detector, $R(\lambda)$, and the black body radiation function, $P(\lambda)$, where λ is the wavelength of the radiation.

$$v(T, T_o) = AA_D\mathcal{J}\int_{1\mu m}^{5.5\mu m} R(\lambda)[P(\lambda, T)\epsilon(\lambda, T) - P(\lambda, T_o)\epsilon(\lambda, T_o)]d\lambda \qquad (6)$$

where A is the amplification, A_D is the detector area and $\mathcal{J}$ is the fraction of energy transmitted

to the detectors by the optical system (related to the aperture). This relation when evaluated for InSb detectors produces a nearly linear relation on a log-log plot(Zehnder and Rosakis, 1991 and 1992). By simply heating a specimen, measuring its surface temperature with a thermocouple, and plotting the results on a log-log plot, one may establish a calibration curve for the detectors that eliminates the need to evaluate the emissivity of the sample, the spectral response of the detector and the black body radiation function. Using this calibration, the voltage record of a detector during a test may be trivially converted into a temperature measurement.

In order to protect the infrared detector imaging system from the dangers of impact loading, dynamic cracks are produced by statically wedge loading a compact tension specimen with a blunt notch. The speed of the crack can be roughly controlled by changing the radius at the notch tip; a blunt notch produces a faster crack than a sharp notch. Dynamic cracks are produced by the storage of elastic energy at the notch tip prior to failure; as the load is increased more elastic energy is stored in the specimen. When a small crack initiates at the notch tip, the excess elastic energy drives the crack dynamically through the specimen. The notch radius is machined by conventional EDM techniques giving a reproducible notch root radius. A minimum radius of .25 mm is attainable resulting in a minimum crack speed of 600 m/s. Crack speed is measured by a series of conducting break-lines on the back surface of the sample. (See Zehnder and Rosakis, 1991 and 1992, and Zehnder and Kallivayalil, 1991) Alternatively, dynamic cracks may also be produced in three point bend impact (Kalthoff, 1985), or mode-II impact loading (Kalthoff, 1987, Lee and Freund, 1990 and Mason et al., 1992).

3. Results and Discussion

The results of four testing conditions are reviewed here. In Fig 2a the results of Zehnder and Rosakis (1991) are recalled, and in Fig 2b the results of a recent investigation by the authors are shown. The material in both experiments is the same, oil-quenched 4340 steel with hardness R_c =44 (See Tables I-III), but the crack speed is 900 m/s in the Zehnder and Rosakis (1991) experiment while the crack speed is 600 m/s here. These results are representative of a number of experiments. In the latter case four separate experiments were performed, some with different apertures, to show the repeatability of the results. Temperature rises below 50°C fall below the noise level of the system. It can be seen that the two fields are significantly different. Most noticeable is the triangular arrangement of the temperature contours behind the crack when

$\dot{a}$ =900 m/s. Contours emanating from the crack tip expand outward initially before curving back to meet the negative x_1 axis. Similar contours are not seen for $\dot{a}$ =600 m/s or in Fig 1. At 600 m/s an interesting feature of the temperature field is seen along the horizontal line, x_2 =1.2. Here the temperature rise due to the formation of another "shear lip" is observed. This formation occurs behind the crack tip and is much less intense in terms of plastic work rate density. Examination of the specimen after failure reveals that the "other shear lip" follows a path parallel to the crack path. The maximum temperature for 900 m/s is 450°C while the maximum temperature for 600 m/s is 300°C. The crack tip positions are estimat d from the crack tip displacement record. This method is not very accurate and the crack tip location uncertainty may be as much as .5 mm.

In Fig 3 the results of some experiments on two separate titanium alloys are shown. In the first case a Ti-10V-2Fe-3Al alloy was tested in the 0%-α state (Giovanola, 1989) (See Tables I-III.) The crack speed is 380 m/s and the maximum temperature is greater than 400°C (the detectors saturated). In the second case the results of Zehnder and Kallivayalil (1991) for Beta-C titanium are shown. The crack speed is 400 m/s, and the maximum temperature is 260°C. The results for Ti-10V-2Fe-3Al bear resemblance to the results for 4340 at 600 m/s as well as the theoretical result shown in Fig 1. Contours extend directly back from the plastic zone roughly parallel to the crack faces eventually curving in to meet at the negative x_1 axis. In contrast, the contours in the experiment on Beta-C titanium emanate outwardly as for 4340 steel at 900 m/s. Further, the existence of a shear localization above the crack tip due to the stress state at the surface of the specimen (Zehnder and Rosakis, 1991) is seen. This "other shear lip" is seen to curve out of the field of view behind the crack tip unlike the "other shear lip" observed in the experiments on 4340 steel at 600 m/s. The shear lips formed in the testing of Beta-C titanium are much smaller than those formed in the testing of Ti-10V-2Fe-3Al. In the Beta-C it can be seen in the figure that the shear lips are approximately .5 mm wide while in Ti-10V-2Fe-3Al examination after testing reveals that the shear lips can be as much as 4 mm wide.

Fractographic analysis of the shear lips offers some interesting comparisons. In Fig 4 the fracture surface of the steel specimen at $\dot{a}$ =600 m/s may be seen both in the flat fracture regime and in the shear lip. It can be seen that there is a drastic difference in the two surfaces. In the flat fracture regime, the surface is rough and the crack path is tortuous. Regions of microvoid coalescence may be observed. On the shear lip, smooth surfaces dominate. This fracture is

similar to the fracture surface reported by Giovanola (1988a and 1988b) for a shear band in the same material with a different heat treatment. Giovanola reports the existence of "cobbled regions" as well as microvoid coalescence regions that are not seen here, but it is clear that the two fracture modes are the same. In the titanium, Fig 5, the flat fracture regime exhibits a tortuous crack path with regions of microvoid coalescence visible along the walls of the peaks and valleys, but in the shear lip fracture is dominated by microvoid coalescence. The voids on the shear lip are much larger than those in the bulk fracture region. None-the-less, it is clear that microvoid coalescence in shear is important in both regions. Thus, the two regions are similar.

3.1 Temperature Fields in Steel

The most striking difference between Figs 2a and 2b is the existence of triangular contours emanating from the crack tip in the temperature field at the higher velocity. Because the velocity of the crack is extremely high when compared to the material properties (the size of the plastic zone and $k/\rho c_p$) in both figures it is expected that *both* fields should reflect the qualitative behavior exhibited in Fig 1 (Mason and Rosakis, 1992). The contour lines should extend directly back from the plastic zone parallel to the crack faces until they eventually curve toward the negative x_1 axis some distance behind the crack tip. This behavior *is* seen in Fig 2b, but it is *not* seen in Fig 2a.

Owing to the heavy dependence of theoretical maximum temperatures upon the assumptions about the plastic zone, it was initially thought that the difference in contours between Figs 2a and 2b might be due to a difference in plastic zone. Unfortunately, estimates of the plastic zone show no difference between the plastic deformation at high and low velocities that could explain the change in the contours. Further, attempts to explain the difference in temperature field at high and low velocities using hyperbolic heat conduction have shown that this theory is not effective in modelling the observed behavior (Mason and Rosakis, 1992). It seems that the change in temperature field at the higher velocities is due to movement of the crack faces. It has been shown by Freund (1977) that, qualitatively, the crack opening velocity should be proportional to the crack velocity and the initial crack tip stress intensity factor. Clearly the crack tip velocity is higher in one case, but, also, the initial stress intensity factor may be as much as three times higher when $\dot{a} = 900$ m/s than when $\dot{a} = 600$ m/s (Rosakis and Zehnder, 1985). Combined, these two effects predict that the crack opening velocity in the 900 m/s test may be 5

times higher than that in the 600 m/s test. From the angle of the contours it is estimated that the average velocity of the crack faces in the x_2 direction is 7.5 m/s when the crack tip velocity is 900 m/s and less than 2 m/s when the crack tip velocity is 600 m/s resulting in a ratio of crack face velocities greater than 4. Inaccuracies are expected when comparing this simple theory with the experimental results. The specimen is much more complex in the experiment than in the theory and measurements of th initiation stress intensity factor were not made. Consequently, it is concluded here that crack opening is responsible for the change in temperature field at the higher velocity, however, no quantitative analysis of this effect is implied.

The plastic work rate ahead of the crack tip may be estimated by using Eq (3) and neglecting conduction (Zehnder and Rosakis, 1991 and 1992, and Zehnder and Kallivayalil, 1991). Letting $\alpha = 0$ in this equation yields

$$-\rho c_p \dot{a} \frac{\partial T}{\partial x_1} = \beta \sigma_{ij} \dot{\epsilon}^p_{ij}. \tag{7}$$

Solving this relation for the experimental results in Fig 2 gives the results shown in Fig 6. For steel β is taken to be .9; this choice is justified by some preliminary results of a split-hopkinson pressure bar investigation of this material parameter (Mason et al., 1992). It is seen that the plastic zone is approximately twice as large in the lower velocity experiment as it is in the higher velocity experiment. The fact that they are almost exactly twice as large in the x_2 direction is due to discretization of the temperature field by the finite detectors. It can only be said that at the lower velocity there is a larger plastic zone then at the higher velocity. The maximum plastic work density rate in the high speed test is 600×10^{12} J/m^{3}s while in the low speed test the maximum is 200×10^{12} J/m^{3}s, a third as much. The change in maximum plastic work rate density and the change in the x_2 dimension of the plastic work zone in conjunction with the fractography seen in Fig 4 indicate that the shear lip is actually a shear band. A localization of the deformation is observed as crack velocity increases indicating the formation of an adiabatic shear band.

Estimation of the energy fraction consumed by the formation of the shear lips (Zehnder and Rosakis, 1991) shows that roughly the same fraction of energy is expended in the shear lips in both the high and low speed experiments. Values for the energy expended in the lips during low speed fracture were, in general, slightly high than the high speed experimental results, but, within the large uncertainty of the calculation, the two are equal. Regardless, a surprisingly large percentage, 50%, of the energy of dynamic fracture is expended in the shear lips during

fast fracture. This is surprising because the area of the shear lips accounts for only about 10% of the fracture surface area in both experiments.

3.2 Temperature fields in Titanium

In titanium the plastic zone is quite similar in size and shape to the plastic zones in steel; see Fig 7. The maximum plastic work rate density at 380 m/s is estimated—since the detectors saturated—to be approximately equal to the maximum plastic work rate density in 4340 steel at 600 m/s while the maximum temperature is greater than 400°C in Ti compared to 300°C in steel. Since adiabatic conditions apply at the crack tip (this is readily shown by comparing the magnitude of two terms on the left hand side of Eq (3)), it is expected that Eq (7), which has no dependence upon thermal conductivity, k, should apply. Thus, the temperatures are *higher* in Ti than in steel when plastic work rates are roughly equal, however they are not higher because of the lower thermal conductivity. The temperature is actually higher because the factor $\rho c_p \dot{a}$ is smaller in the titanium; in titanium $\rho c_p \dot{a} = 8.7 \times 10^8$ J/m^{2}s°C while in steel $\rho c_p \dot{a} = 21.0 \times 10^8$ J/m^{2}s°C, roughly twice that in titanium.

Bryant et al. (1986) indicate evidence of localized melting in the Ti-10V-2Fe-3Al alloy used here, but fractographic examination in Fig 5 gives no indication of melting in the shear lips or the flat fracture region. This may be due to differences in heat treatment.

In the experiments by Zehnder and Kallivayalil (1991) on Beta-C titanium the existence of a shear lip above the actual crack demonstrates that crack face opening has an effect on the measurement of temperature field. The shear lip is seen to curve out of the field of view. Since it is certain that near adiabatic conditions apply and that shear lip formation occurs parallel to the crack path, it is concluded that this movement is due to a translation of the crack faces rather than a change in the deformation. Thus, crack face opening effects are seen in Beta-C titanium at 400 m/s supporting the conclusion that crack face opening is seen in the steel tests at 900 m/s.

4. Conclusions

1. It is clear that the shear lip formed in oil-quenched 4340 steel is actually a shear band, a localization of the shear deformation to a narrow plane as a result of thermal softening in the material. At lower velocities the localization is less pronounced and

the maximum temperature measured is lower. Fractography indicates a shear band fracture mode in the shear lip but not in the flat fracture regime.

2. The temperature field around a dynamically propagating crack tip in oil-quenched 4340 steel changes significantly when the crack velocity is increased from 600 m/s to 900 m/s. This effect is attributed to the faster crack opening rate at higher velocities. Conclusive evidence of crack face opening is seen in the temperature fields of Zehnder and Kallivayalil for Beta-C titanium (Zehnder and Kallivayalil, 1991), and it is predicted by a simply theory that crack face opening will be much more significant at 900 m/s than at 600 m/s in 4340 steel.

3. In titanium the generation of heat at the tip of a dynamically propagating crack has been investigated. The maximum temperature in Ti-10V-2Fe-3Al for equivalent maximum plastic work rate densities is higher than in 4340 steel. Because of the adiabatic conditions at the crack tip this effect is not attributed to the lower thermal conductivity, rather it is attributed to lower crack speeds, the lower density and the lower heat capacity of titanium though the factor $\rho c_p \dot{a}$.

4. In Ti-10V-2Fe-3Al in the shear lips, failure is dominated by nucleation and growth of large micro-voids while in the bulk, flat-fracture region, failure occurs by the nucleation and growth of smaller micro-voids and a more tortuous crack path. Large micro-voids generate more plasticity than small voids, so it is expected that temperatures will be higher when microvoid growth is more extensive, in the shear lip.

Acknowledgements

We are grateful to A.T. Zehnder for sharing the raw data from his investigation and to J. Kallivayalil and A.T. Zehnder for sharing figures from their work together. The computations described here were carried out on a Cray Y-MP at the San Diego Supercomputing Center (SDSC).

References

1. *Aerospace Structural Metals Handbookm (1989)*, Metals and Ceramics Information Center, Battelle Columbus Laboratories, Columbus, Ohio, Vol. 1, code 1206

2. M.B. Bever, D.L. Holt and A.L. Titchener (1973), The stored energy of cold work, *Prog. Mat. Sci.*, **17**, 1

3. J.D. Bryant, D.D. Makel and H.G.F. Wilsdorf (1986), Observations on the effect of temperature rise at fracture in two titanium alloys, *Mat. Sci. Engr.*, **77**, 85,

4. H.S. Carslaw and J.C. Jaeger (1959), *Conduction of Heat in Solids*, Oxford Press, London

5. R.J. Clifton and R.W. Klopp (1985), Pressure-shear plate impact testing, *Metals Handbook; 9th Edition*, American Society for Metals, Metals Park, OH, Vol. 8, 230

6. C.S. Coffey and S.J. Jacobs (1981), Detection of local heating in impact or shock experiments with thermally sensitive films, *J. Appl. Phys.*, **52**, 6991

7. W. Döll (1973), An experimental study of the heat generated in the plastic region of a running crack in different polymeric materials, *Engr. Frac. Mech.*, **5**, 259

8. A.S. Douglas and H.U. Mair (1987), The temperature-field surrounding a dynamically propagating mode-III crack, *Scripta Met.*, Vol. 21, p. 479, 1987

9. J. Duffy (1984), Temperature measurements during the formation of shear bands in a structural steel, G.J. Dvorak and R.T. Shield, eds., *Mechanics of Material Behavior*, Elsevier Science Pub. B.V., Amsterdam, 75

10. I.M. Egdall (1985), Manufacture of a three mirror wide-field optical system, *Optical Engr.*, **24**, 285

11. P.S. Follansbee (1985), The split hopkinson bar, *Metals Handbook; 9th Edition*, American Society for Metals, Metals Park, OH, **8**, 198

12. P.G. Fox and J. Sonria-Ruiz (1970), Fracture-induced thermal decomposition in brittle crystalline solids, *Proc. R. Soc. London A*, **317**, 79

13. L.B. Freund (1977), A simple model of the double cantilever beam crack propagation specimen, *J. Mech. Phys. Sol.*, **25**, 69

14. K.N.G. Fuller, P.G. Fox and J.E. Field (1975), Temperature rise at the tip of fast moving cracks in glassy polymers, *Proc. Roy. Soc. London A*, **341**, 537

15. J.H. Giovanola (1988a), Adiabatic shear banding under pure shear loading, Part I., *Mechanics of Materials*, **7**, 59

16. J.H. Giovanola (1988b), Adiabatic shear banding under pure shear loading, Part II., *Mechanics of Materials*, **7**, 73

17. J.H. Giovanola, R.W. Klopp and J.W. Simons (1989), Effect of shear lips on dynamic crack propagation, *Proc. OJI International Seminar on Dynamic Fracture*, Toyohashi, Japan, August, 1989

18. K.A. Hartley, J. Duffy and R.H. Hawley (1987), Measurement of the temperature profile during shear band formation in steels deforming at high strain rates, *J. Mech. Phys. Sol.*, **35**, 283

19. J.W. Hutchinson (1984), Introduction to the viewpoint on shear bands, *Scripta Met.*, **18**, 421

20. J.F. Kalthoff (1985), On the measurement of dynamic fracture toughnesses—a review of recent work, *Int. J. Frac.*, 27, 277

21. J.F. Kalthoff (1987), Shadow optical analysis of dynamic shear fracture, *Photomechanics and Speckle Metrology*, SPIE Vol. 814, 531

22. W. Klemm (1989), *presented at the Joint American Society of Mechanical Engineers, Japan Society of Mechanical Engineers International Pressure Vessel and Piping Conference*

23. R. Krishna Kumar, R. Narasimhan and O. Prabhakar (1991), Temperature rise in a viscoplastic material during dynamic crack growth, *Int. J. Fracture*, **48**, 23

24. Z.-B. Kuang and S. Alturi(1985), Temperature field due to a moving heat source: a moving mesh finite element analysis, *J. Appl. Mech*, **52**, 277

25. Y.J. Lee and L.B. Freund (1990), Fracture initiation due to asymmetric impact loading of an edge cracked plate, *J. Appl. Mech.*, **57**, 104

26. Z.L. Li, J.L. Yang and H. Lee (1988), Temperature fields near a running crack tip, *Eng. Frac. Mech.*, **30**, 791

27. P.N. Malali (1988), Thermal Fields Generated by Dynamic Mode III Fracture in Ductile Materials, M.S. Thesis, The Johns Hopkins University, Baltimore, 1988

28. A. Marchand and J. Duffy (1988), An experimental study of the formation process of adiabatic shear bands in a structural steel, *J. Mech. Phys. Sol.*, **36**, 251

29. J.J. Mason, J. Lambros and A.J. Rosakis (1991), On the use of a coherent gradient sensor in dynamic mixed-mode fracture mechanics experiments, to appear *J. Mech. Phys. Sol.*

30. J.J. Mason and A.J. Rosakis (1992), The effect of hyperbolic heat conduction around a dynamically propagating crack tip, SM Report 92-3, Graduate Aeronautical Laboratories, California Inst. of Tech.

31. J.J. Mason, A.J. Rosakis and G. Ravichandran, The conversion of plastic work to heat around a dynamically propagating crack in metals, SM Report 92-17, Graduate Aeronautical Laboratories, California Inst. Tech., Pasadena, CA 91125, 1992

32. *Metals Handbook, 9th Edition* (1980), American Society for Metals, Metals Park, OH, Vol. 3, 397

33. G.L. Moss and R.B. Pond (1975), Inhomogeneous thermal changes in copper during plastic elongation, *Met. Trans. A*, **6A**, 1223

34. A. Offner (1975), New concepts in projection mask aligners, *Optical Engr.*, **14**, 130

35. S.Y. Rah and S.S. Lee (1989), Four-spherical-mirror zoom telescope continuously satisfying the aplanatic condition, *Optical Engr.*, **28**, 1014

36. J.R. Rice and N. Levy (1969), Local heating by plastic deformation at a crack tip, in A.S. Argon, ed., *Physics of Strength and Plasticity*, M.I.T. Press, Cambridge, MA, 277

37. A.J. Rosakis and A.T. Zehnder (1985), Dynamic fracture initiation and propagation in 4340 steel under impact loading, *Int. J. Frac.*, Vol. 27, p. 169, 1985

38. D.A. Schokey, J.F. Kalthoff, W. Klemm and S. Winkler (1983), Simultaneous measurements of stress intensity and toughness for fast cracks in steel, *Exp. Mech.*, **40**, 140

39. I.N. Sneddon and D.S. Berry (1958), The classical theory of elasticity, in S. Flugge, ed., *Handbuch der Physik*, Vol VI, Springer-Verlag, Berlin, 123

40. J.C. Sung and J.D. Achenbach (1987), Temperature at a propagating crack tip in a viscoplastic material, *J. Thermal Stresses*, **10**, 243

41. A. Suzuki (1983a), Complete analysis of a two-mirror unit magnification system, Part I., *Appl. Optics*, **22**, 3943

42. A. Suzuki (1983b), Complete analysis of a two mirror unit magnification system, Part II., *Appl. Optics*, **22**, 3950

43. G.M. Swallowe, J.E. Field and L.A. Horn (1986), Measurements of transient high temperatures during the deformation of polymers, *J. Mat. Sci.*, **26**, 4089

44. G.I. Taylor and M.A. Quinney (1934), The latent energy remaining in a metal after cold working, *Proc. Roy. Soc London A*, **143**, 307

45. D.Y. Tzou (1990a), Thermal shock waves induced by a moving crack, *J. Heat Transfer*, **112**, 21

46. D.Y. Tzou (1990b), Thermal shock waves induced by a moving crack—a heat flux formulation, *Int. J. Heat Transfer*, **33**, 877

47. R. Weichert and K. Schönert (1974), On the temperature rise at the tip of a fast running crack, *J. Mech. Phys. Sol.*, **22**, 127

48. R. Weichert and K. Schönert (1978a), Temperature distribution produced by a moving heat source, *Q. J. Mech. Appl. Math.*, **31**, 636

49. R. Weichert and K. Schönert (1978b), Heat generated a the tip of a moving crack, *J. Mech. Phys. Sol.*, **26**, 151

50. A.T Zehnder and A.J. Rosakis (1991) On the temperature distribution at the vicinity of dynamically propagating cracks in 4340 steel, *J. Mech. Phys. Sol.*, **39**, 385

51. A.T. Zehnder and A.J. Rosakis (1992), Temperature rise at the tip of dynamically propagating cracks: measurements using high speed infrared detectors, to appear *Experimental Mechanics in Fracture*, **III**

52. A.T. Zehnder and J.A. Kallivayalil (1991), Temperature rise due to dynamic crack growth in Beta-C titanium, *Speckle Techniques, Birefringence Methods, and Applications to Solid Mechanics*, SPIE Vol. 1554A, 48

Table I: Tensile Properties				
Material and Condition	σ_y MPa	σ_u MPa	ϵ_u %	K_{Ic} MPa$\sqrt{m}$
4340, quenched[50]		1700		44
Ti, 0%—α[17]	1370	1390	0.35	56

Table II: Elastic Properties			
Material and Condition	E GPa	ν	ρ kg/m^3
4340, quenched[1]	210	.30	7830
Ti, 0%—α[3,32]	110	.32	4650

Table III: Thermal Properties				
Material and Condition	c_p J/kg°C	k W/m°C	α μm^2/s	κ μm/m°C
4340, quenched[1]	448	34.6	9.86	11.2
Ti, 0%—α[3,32]	490	10.9	4.78	9.7

(Values are taken from the indicated reference number.)

List of Figures

Figure 1 Theoretical calculation of the temperature field around a propagating crack tip in steel (Mason and Rosakis, 1992). A convolution of the the form in Eq (5) is used in conjunction with an approximation to the experimentally measured plastic work zone shown in Figs 6 and 7.

Figure 2 Temperature distribution measured experimentally using infrared detectors around a crack tip propagating in 4340 oil quenched steel at a velocity of 900 m/s (Zehnder and Rosakis, 1991) and 600 m/s. Maximum temperatures of approximately 450°C at 900 m/s and 300°C at 600 m/s are observed. The crack line location in the vertical direction is estimated from the symmetry of the results. The temperature rise at $x_2 \approx 1.2$ mm in the slower velocity experiment is due to the formation of another shear lip. Note that this formation occurs behind the crack tip at distances at least as large as 20 mm.

Figure 3 The temperature field around a crack tip propagating at 380 m/s in Ti-10V-2Fe-3Al alloy and 400 m/s in Beta-C Ti (Zehnder and Kallivayalil, 1991). Some of the detectors were saturated in the Ti 10V-2Fe-3Al test, but a maximum temperature of approximately 500°C may be extrapolated from the results. In the Beta-C Ti material a maximum temperature of 260°C is reported.

Figure 4 Examination of the fracture surfaces in steel reveals different fracture morphology (a) in the flat fracture region than (b) on the shear lips. The smoother fracture surface in the shear lips indicates the formation of a shear band as seen in Giovanola (1988a and 1988b).

Figure 5 The fracture surfaces in Ti-10V-2Fe-3Al reveal very similar fracture in (a) the flat fracture region and (b) the shear lip. However, more evidence of ductile void growth is evident in the shear lip and a more tortuous path is seen in the flat fracture regime.

Figure 6 The plastic work zone as estimated from Eq (7) is shown for a crack propagating in oil-quenched 4340 steel at two velocities; 900 m/s and 600 m/s. It is seen that the plastic zone is elongated in the x_1 direction and that although the shape is the same at both velocities the zone at higher velocities is smaller reflecting a localization of plastic deformation as velocity increases.

Figure 7 The plastic zone for Ti-10V-2Fe-3Al is estimated as in Eq (7). The zone shows similarity in shape to the results for 4340 steel in Fig 6. The magnitude of the plastic work is the same as for oil quenched 4340 steel with a crack propagating at 600 m/s, but the temperature is higher because the factor $\rho c_p \dot{a}$ is smaller in the Ti-10V-2Fe-3Al.

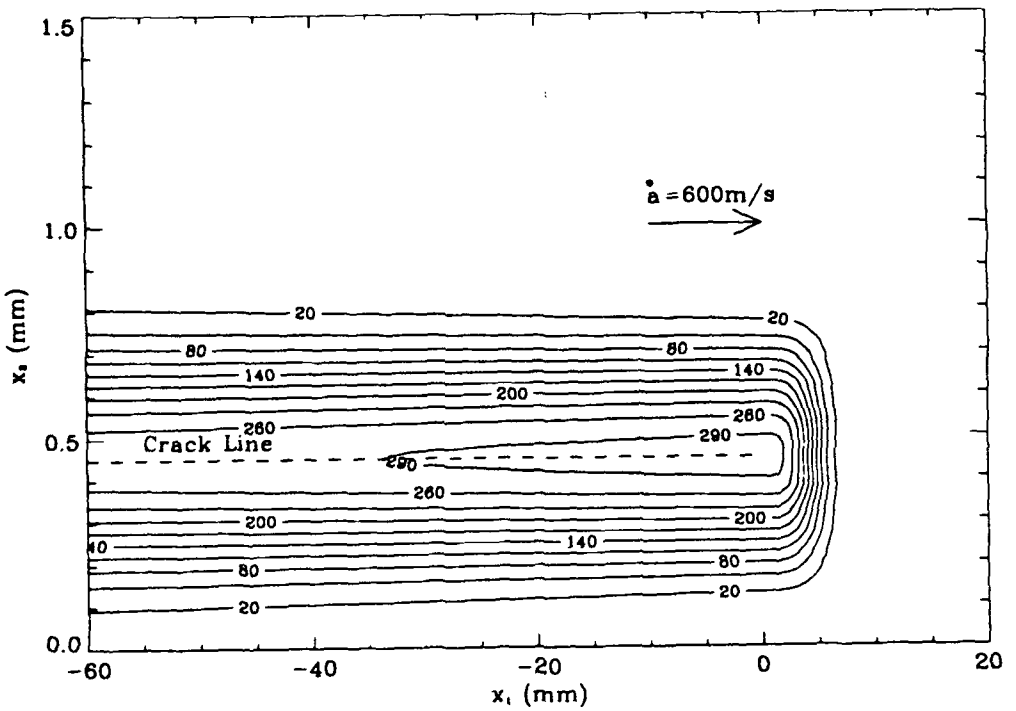
1.5
1.0
0.5
0.0
x_2 (mm)
$\dot{a}$ =600m/s
Crack Line
20
80
140
200
260
290
-60
-40
-20
0
20
x_1 (mm)

FIGURE 1

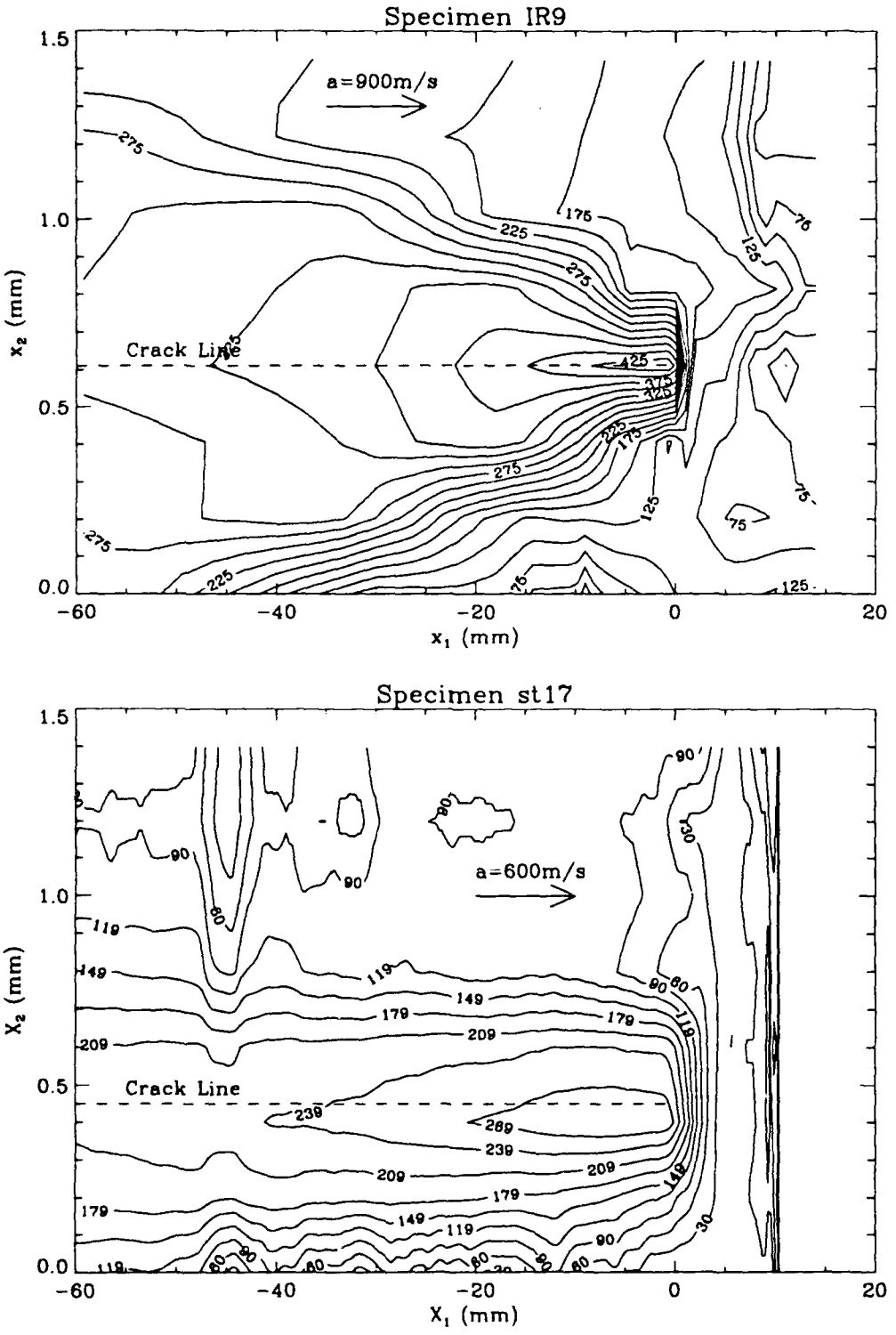
Specimen IR9
a=900m/s
Crack Line
x_2 (mm)
x_1 (mm)
Specimen st17
a=600m/s
Crack Line
X_2 (mm)
X_1 (mm)

FIGURE 2

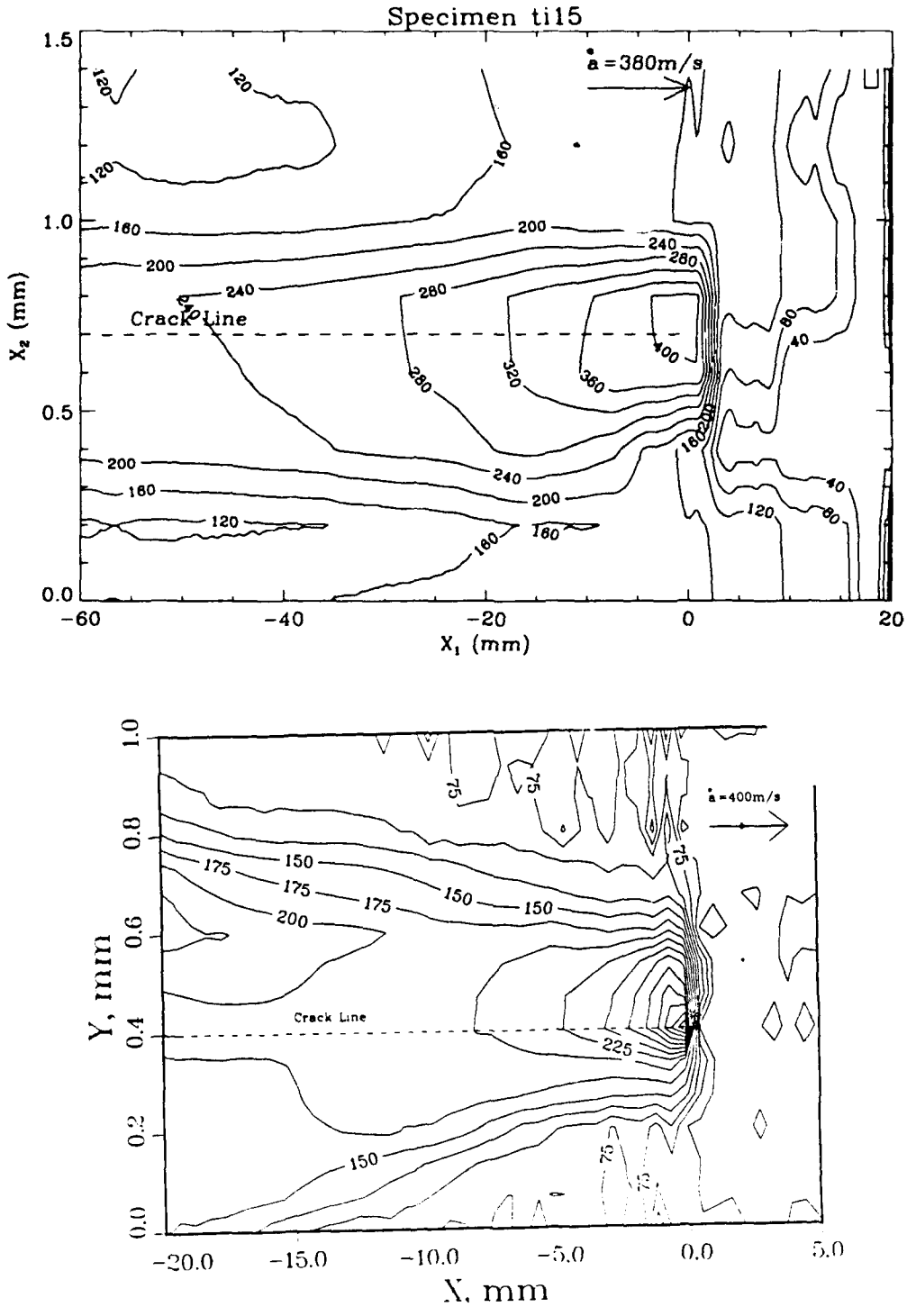
Specimen ti15
ȧ =380m/s
Crack Line
X₂ (mm)
X₁ (mm)
ȧ =400m/s
Crack Line
Y, mm
X, mm

FIGURE 3

(a)

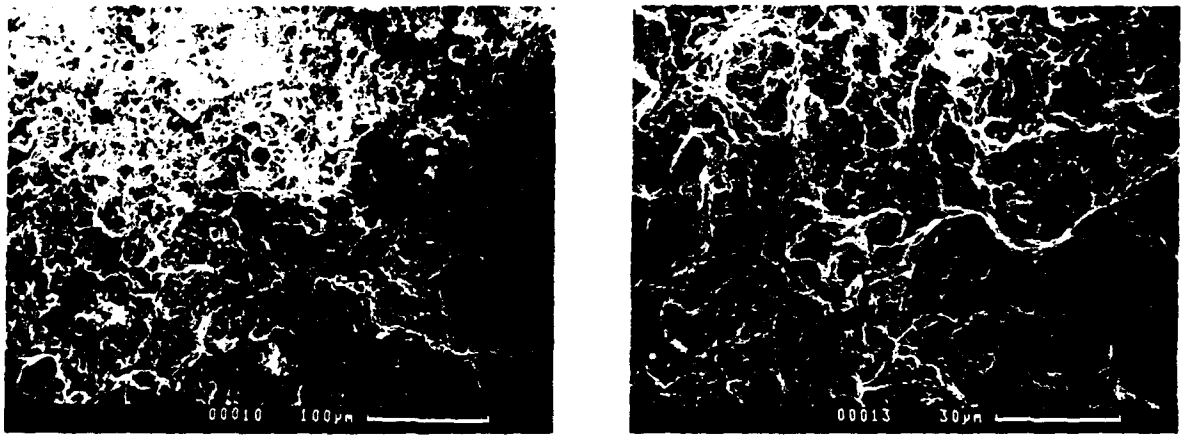

(b)

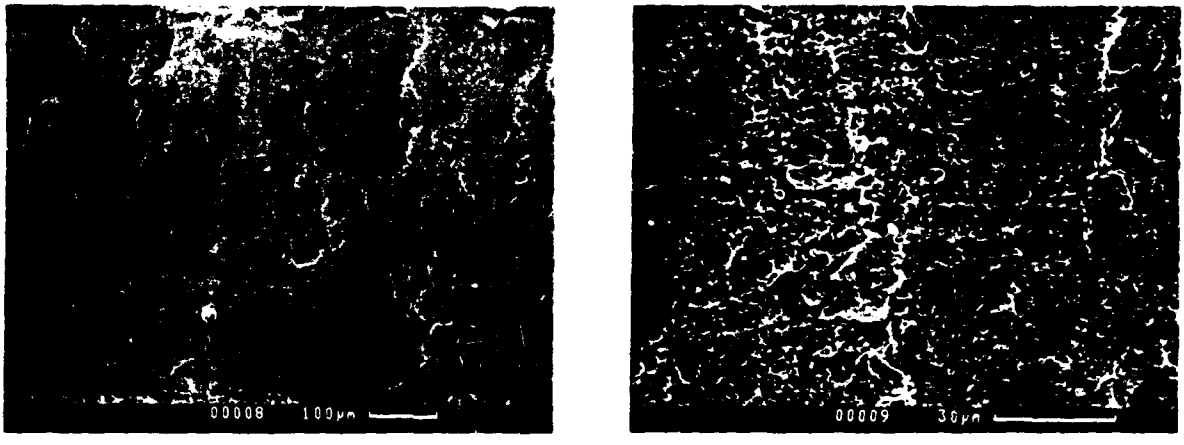

FIGURE 4

(a)

(b)

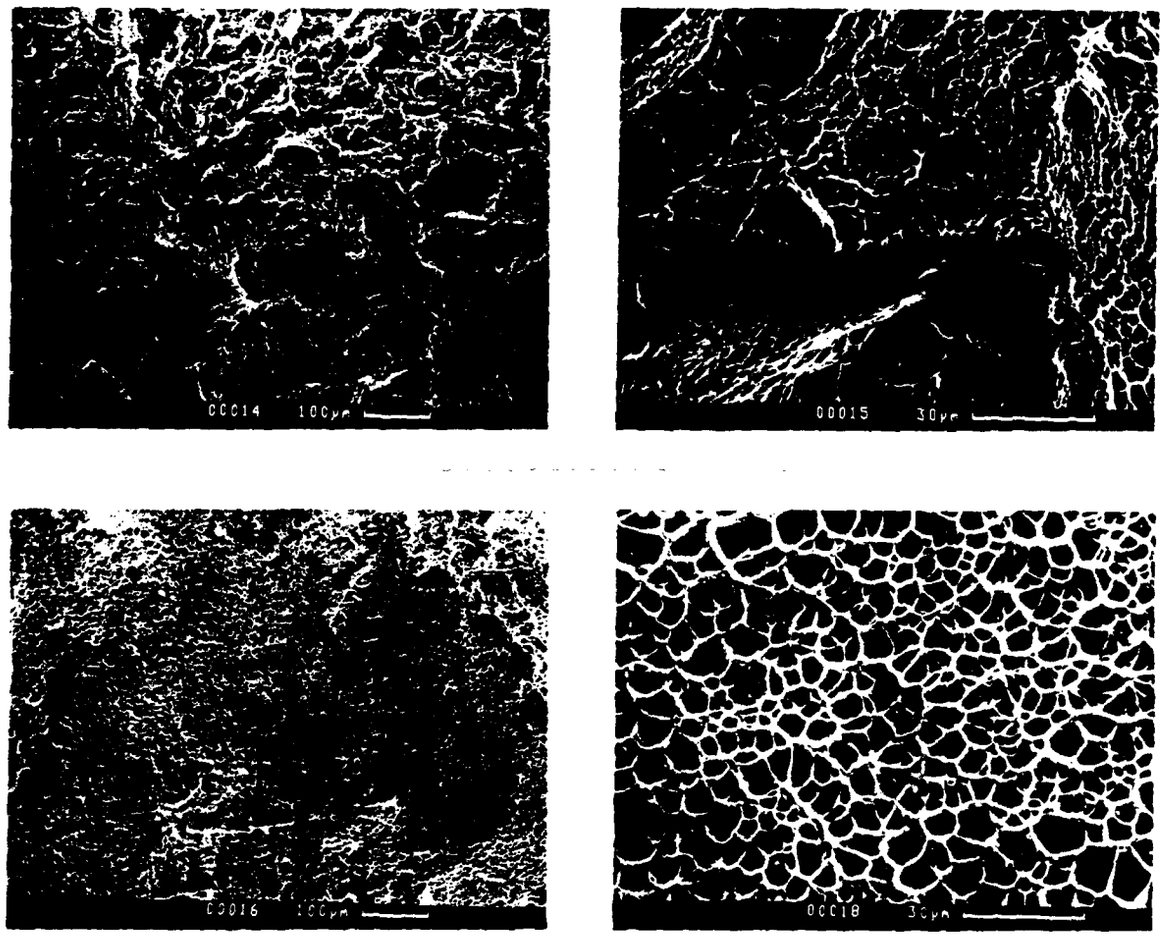

FIGURE 5

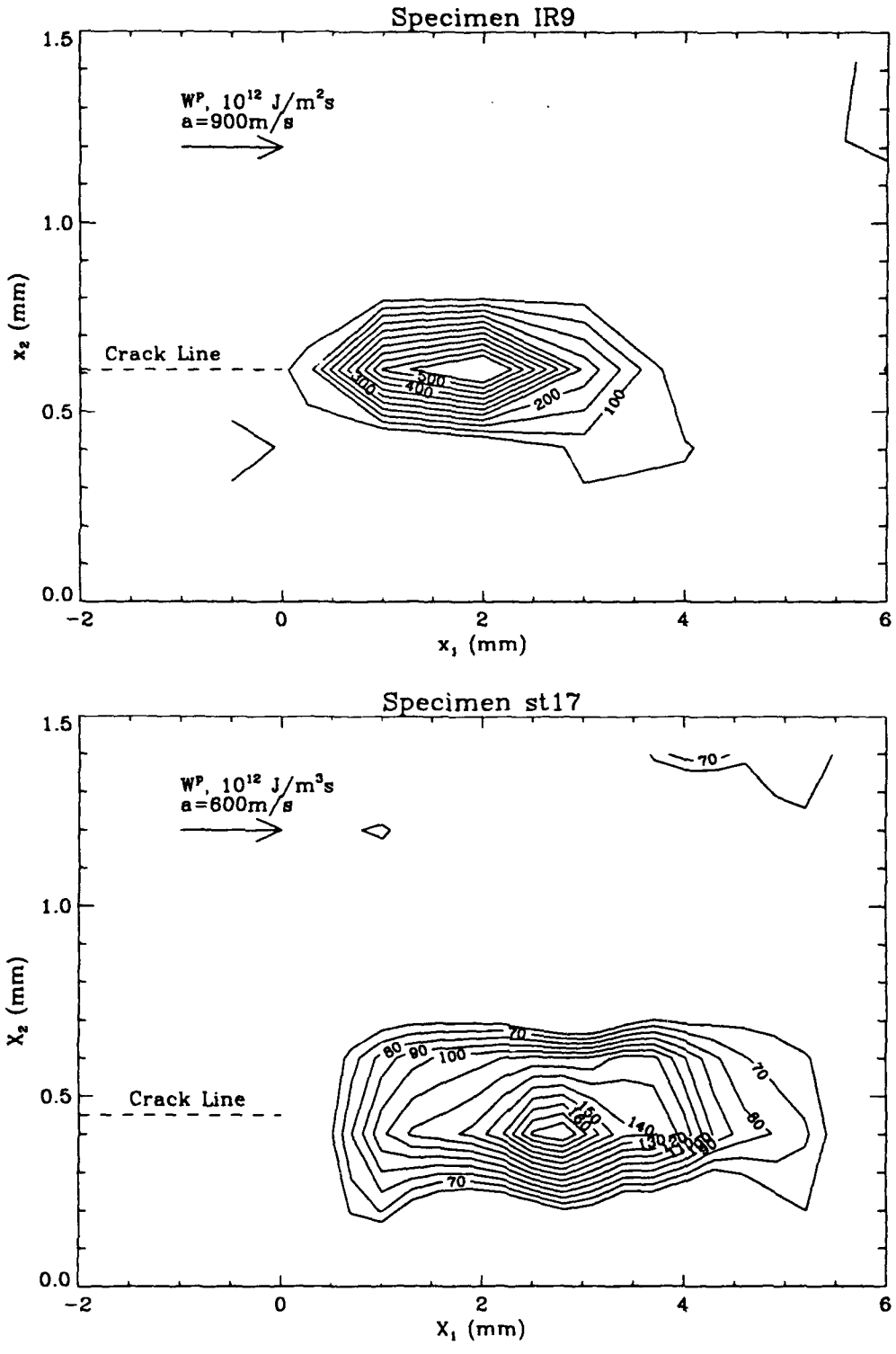
Specimen IR9
W^P, 10^{12} J/m^{2}s
a=900m/s
Crack Line
300
400
500
200
100
x_2 (mm)
x_1 (mm)
1.5
1.0
0.5
0.0
−2
0
2
4
6
Specimen st17
W^P, 10^{12} J/m^{3}s
a=600m/s
Crack Line
70
80
90
100
150
140
130
120
110
X_2 (mm)
X_1 (mm)

FIGURE 6

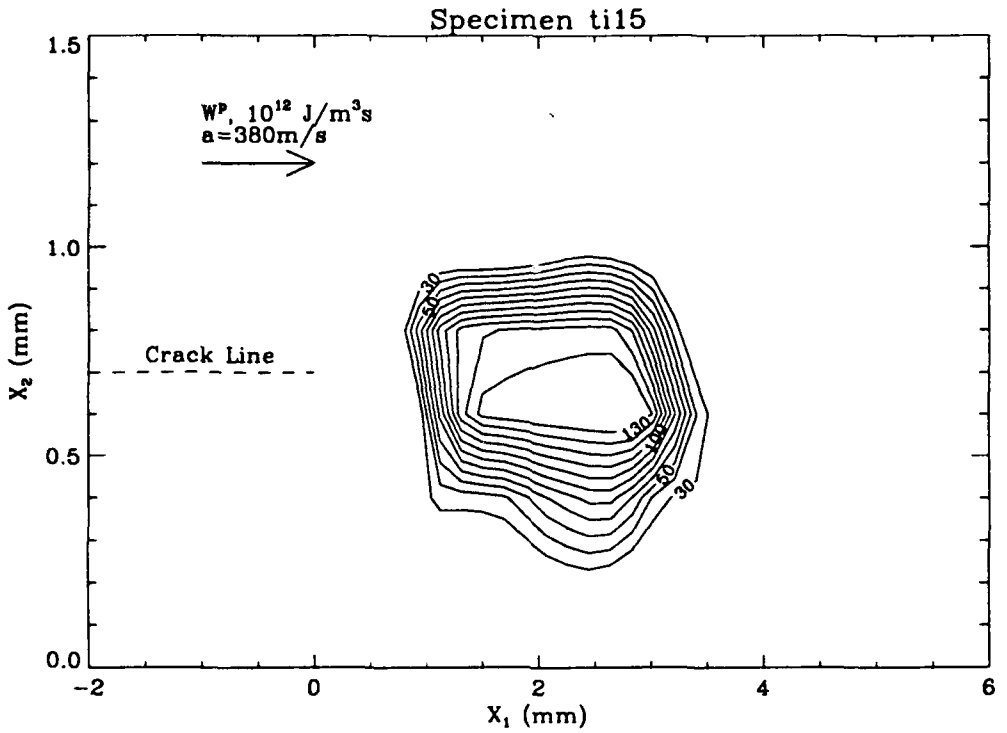
Specimen ti15
W^p, 10^{12} J/m^{3}s
a=380m/s
Crack Line
1.5
1.0
0.5
0.0
X_2 (mm)
−2
0
2
4
6
X_1 (mm)
30
50
70
100
130

FIGURE 7